Closing the budget of 20th Century True Polar Wander

Siavash Ghelichkhan[1], Kimberly M. Moore[2], Mark J. Hoggard[1],
Fred D. Richards[3], Ngai-Ham Chan[4], Jessica R. Creveling[5], Jerry X. Mitrovica[6]

[1]Research School of Earth Sciences, Australian National University
[2]Division of Geological and Planetary Sciences, California Institute of Technology
[3]Royal School of Mines, Imperial College London
[4]Helmholtz Centre Potsdam - The GFZ German Research Centre for Geosciences
[5]College of Earth, Ocean, and Atmospheric Sciences, Oregon State University
[6]Department of Earth & Planetary Sciences, Harvard University

Abstract

We revisit the budget of 20th century true polar wander (~1°/Myr in the direction of 70°W) using a state-of-the-art adjoint-based reconstruction of mantle convective flow and predictions of ongoing glacial isostatic adjustment (GIA) that adopt two independent models of Pleistocene ice history. Both calculations are based on a mantle viscosity profile that simultaneously fits a suite of GIA-related data sets (Fennoscandian Relaxation Spectrum, post-glacial decay times) and a set of present-day observations associated with mantle convection (long-wavelength gravity anomalies, plate motions, excess ellipticity of the core-mantle-boundary). Our predictions reconcile both the magnitude and direction of the observed TPW rate, with convection and GIA contributing signals that are 25-30% and 75-80% of the observed rate, respectively. The former assumes that large-scale seismic velocity heterogeneities are purely thermal in origin, and we argue that our estimate of the convection signal likely represents an upper bound due to the neglect of compositional variations within the Large Low Shear Velocity Provinces in the deep mantle.

Introduction

True polar wander (TPW) refers to the long-term motion of the rotation axis of the Earth relative to the surface geography. A combination of astronomic and geodetic measurements indicates that TPW during the 20th century was characterized by a mean drift of the North Pole toward Québec (~70°W) at a rate of ~1°/Myr (~11 cm/yr; Fig. 1; Argus & Gross, 2004). Beginning in the early 1980s, this signal was assumed to reflect the ongoing adjustment of the Earth in response to the past ice age – a hypothesis consistent with the observed direction of

the polar motion – and models of the glacial isostatic adjustment (GIA) process were compared to the observed rate to infer deep mantle viscosity (e.g., Sabadini & Peltier, 1981; Sabadini et al., 1982; Wu & Peltier, 1984). It was soon recognized that modern climate signals, and in particular the melting of glacier systems, could have a non-negligible impact on TPW (e.g., Peltier, 1988) and studies of this connection came to define "Munk's Enigma". Munk (2000) demonstrated that various observations related to Earth rotation, including TPW, could be reconciled with a standard GIA model, leaving no room for the signal associated with modern glacier or ice sheet melting at a rate implied by estimates global mean sea level (GMSL) rise over the 20th century. Mitrovica et al. (2015) resolved the enigma by adopting an updated (and lower) estimate of 20th century GMSL (Hay et al., 2015), using an improved model of the radial profile of mantle viscosity, and a more accurate treatment of GIA-induced TPW (Mitrovica et al., 2005). Their analysis concluded that GIA was the dominant signal in 20th century TPW, explaining the direction and ~80% of the rate of polar motion.

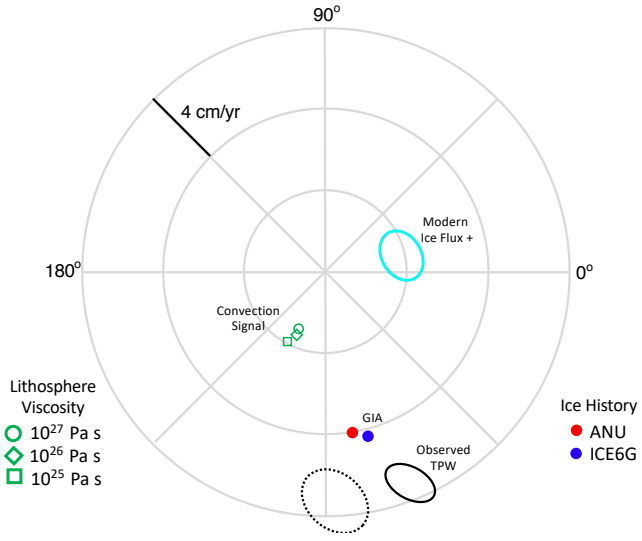

Fig. 1: Observed and predicted 20th century TPW. Black oval (solid line) – observed TPW based on the set of results in Argus and Gross (2004) using hotspot or mean mantle reference frames. The modern ice flux+ (cyan oval), GIA and mantle convection signals

are described in the text. Two GIA simulations distinguished on the basis of the adopted ice history (as labelled, bottom right) are shown. The convection predictions involve three reconstructions distinguished on the basis of the viscosity of the lithosphere (as labelled, bottom left). Black oval (dotted line) – observed TPW minus modern ice mass+ signal. Angles on the perimeter refer to degrees, east longitude.

These various studies neglected the possibility that mantle convective flow, the driving force of plate tectonics, contributed significantly to the TPW over the past century. Steinberger & O'Connell (1997), in contrast, concluded that convection contributed ~40% of the modern TPW rate in the direction of East Greenland, and argued that the signal should be considered in efforts to close the budget of 20th century TPW. Their study was based on backward advection convection schemes in which a present-day mantle density heterogeneity inferred from seismic tomography (Su et al., 1994) was evolved backward in time for tens of millions of years (ignoring thermal diffusion) to establish time series of inertia tensor perturbations. Using the same viscous flow theory, but different models for the mantle density field that combined reconstructions of plate subduction history with density anomalies associated with the two Large Low Shear Velocity Provinces in the deep mantle, Steinberger & Torsvik (2010) estimated TPW rates of 0-0.3°/Myr over the past 10 Myr, generally in the direction of Greenland. These efforts were part of a large body of published work that explored the relatively muted (~10°) history of TPW over the past 120 Myr inferred from paleomagnetic data using rotational stability theories of widely varying levels of sophistication (Ricard et al., 1993; Richards et al., 1997, 1999; Greff-Lefftz, 2004; Steinberger & Torsvik, 2008; Rouby et al., 2010; Chan et al., 2011). A general conclusion from such studies was that long-term rates of TPW in recent geological history were of order 0.1°/Myr (~1.1 cm/yr).

Adhikari et al. (2018) revisited the budget of 20th century TPW considering contributions from GIA, modern melting of ice sheets and glaciers, water impoundment in dams, flux of groundwater between continents and oceans, steric effects and mantle convection. They concluded that a mantle convection signal in TPW with a magnitude of ~50-70% of the observed rate was necessary to reconcile the 20th century trend after correction for the remaining signals. The analysis involved 283 convection simulations using a variety of

approaches, including a tracking of inertia tensor perturbations based on reconstructions of subduction histories or backward advection of initial buoyancy fields computed from a suite of seismic tomography models. The simulations had a mean TPW rate of 0.21° ± 0.01°/Myr, significantly lower than the above bound, and only 5 of the predictions yielded a convection signal that satisfied the TPW observation. The study also concluded that GIA contributed only ~30% of the observed 20th century rate.

Results

Rigorously establishing the magnitude of the mantle convection signal in 20th century TPW is clearly vital for efforts to use the datum to constrain modern global change processes. Figure 1 shows both the observational constraint on TPW (Argus & Gross, 2004; black oval - solid) and the signal associated a suite of processes thought to drive TPW, not including GIA and mantle convection (cyan oval). The latter, computed by Adhikhari et al. (2018), involves contributions from: (1) modern ice mass flux from global glacier systems, the Greenland Ice Sheet, and the Antarctic Ice Sheet; (2) water impoundment in dams; (3) flux of groundwater between continents and oceans; (4) ocean steric effects; and (5) seismic events. The modern ice mass signal (1), which dominates the total, was based on the Randolph Glacier Inventory (RGI Consortium, 2017; Marzeion et al., 2015) derived from climate modeling consistent with observations of glacier volume change and surface mass balance, 20th century Greenland Ice Sheet mass changes estimated from aerial imagery and altimetry measurements (Kjeldsen et al., 2015), and a suite of regional studies of 20th century Antarctic Ice Sheet and glacier changes. The remaining components (2)-(4) yield a net signal of only ~0.3 cm/yr with an uncertainty of ~1 cm/yr.

We henceforth term the total signal from (1)-(5) the modern ice flux+ signal. The observed TPW rate corrected for this signal (Fig. 1, black oval, dashed) is ~11.3 cm/yr (~1°/Myr) directed toward eastern Hudson Bay (-90°E). Absent other unknown process driving significant long term TPW, this signal must originate from a combination of GIA and mantle convection effects. Models of both processes should be based on consistent models of the Earth's viscous structure. In the present study, we adopt the viscosity profile of Mitrovica et al. (2005), which is

within the class of models derived through simultaneous inversion of ice age and mantle convection data sets (Mitrovica and Forte, 2004). The ice age data included a set of observations that are relatively insensitive to uncertainties in ice history, the Fennoscandian Relaxation Spectrum and post-glacial decay times over Hudson Bay and Fennoscandia, while the convection date included long wavelength gravity anomalies, plate motions, surface dynamic topography and the excess ellipticity of the core-mantle-boundary (CMB). The mantle viscosity profile we adopt is characterized by a ~2.5 order of magnitude increase from the base of the lithosphere to the deep mantle, followed by a decrease of comparable amount toward the CMB (Fig. 2).

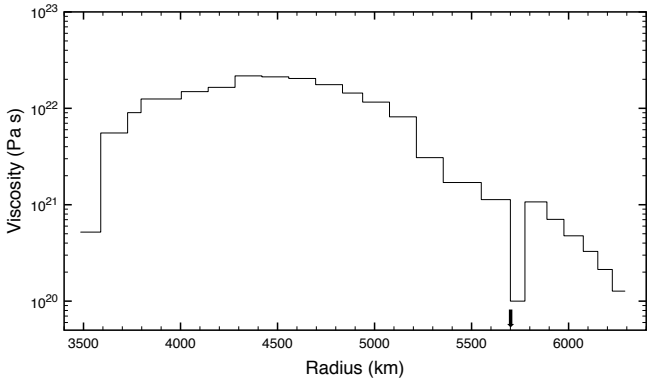

Fig. 2: Mantle viscosity profile adopted in simulations. 23-layer viscosity profile extending from the core-mantle-boundary to the base of the lithosphere, after Mitrovica et al. (2015). Arrow on the x-axis indicates the depth of the boundary between upper and lower mantle.

Our new analysis of the TPW signal due to mantle convection involves several important improvements to previous work. First, and most importantly, the simulations of mantle convection, and its impact on the Earth's inertia tensor, are based on an adjoint methodology that solves the full field equations governing compressible mantle convection, including thermal diffusion (Ghelichkhan & Bunge, 2016, 2018, 2021; see Methods). Adjoint modeling has

two major advantages over the backward advection studies listed above for reconstructing Cenozoic mantle structure and dynamics. The simulations are constrained to fit present-day observations related to the mantle convection process, and they avoid transient behavior that occurs in backward advection schemes. The latter instability contaminates the most recent phase of evolution, which is the time period of interest here. A second improvement involves the rotational stability theory we apply to the inertia time series. Previous studies generally adopted the canonical TPW theory of Gold (1955) and Goldreich and Toomre (1969) in which no stabilization of the rotation axis due to delayed adjustment of the rotational bulge of the Earth is included. Our calculations are based on the treatment of Moore et al. (2017), which includes this stabilization due to the rotational bulge (Ricard et al., 1993) and the so-called "remnant bulge" (Willemann, 1984; Matsuyama et al., 2006) associated with the presence of a (high viscosity) viscoelastic lithosphere (see Methods).

Commented [MOU1]: Sia – Should we cite the observations and the fit to these observations? We could do this in the Methods/Supplement section and simply add a citation to that here.

The adjoint-based reconstructions yield a 50 Myr time series of non-hydrostatic inertia tensor perturbations. All TPW calculations extend 3000 Myr, and begin with a 2950 Myr ramp up in which the inertia tensor stays fixed to the first values computed in the adjoint simulation. The calculations end at the present day. TPW reconstructions adopt the same viscosity profile used in the adjoint simulation and, in addition, we consider three values for lithospheric viscosity: 10^{25} Pa s, 10^{26} Pa s, and 10^{27} Pa s. These values have characteristic relaxation times of 5 Myr, 50 Myr, and 500 Myr, respectively, and the 2950 Myr ramp up ensures that the pole position at 50 Ma is the same in all three cases.

The predicted pole path since 50 Ma (i.e., from the onset on convection-induced perturbations in the inertia tensor) is broadly similar and, as one would expect, the net displacement of the pole decreases as the lithospheric viscosity increases (Fig. 3). The relaxation time of the 10^{25} Pas lithosphere is sufficiently short that any further decrease in viscosity will not impact the pole path (i.e., stabilization is provided by the rotational bulge alone). In contrast, the highest lithospheric viscosity case experiences negligible viscous relaxation in the lithosphere over the 50 Myr convection simulation, and the lithosphere behaves essentially as an elastic plate (i.e.,

stabilization is also provided by the remnant bulge). The computed path approximately follows the meridian 225°E/45°E from ~50-15 Ma, and then turns to follow a southwest path over the subsequent 15 Myr. The present-day TPW rate in these convection simulations increases from 3.3 to 3.9 cm/yr (3.0-3.5°/Myr) as the lithospheric viscosity is decreased from 10^{27} to 10^{25} Pa s, a range that represents ~25-30% of the observed magnitude (Fig. 1). As we have noted, stabilization by the remnant bulge is small for lithospheric viscosities less than 10^{25} Pa s, and thus any further reduction in this viscosity toward the value in the shallow upper mantle (~10^{20} Pa s) has negligible effect on the predicted rate.

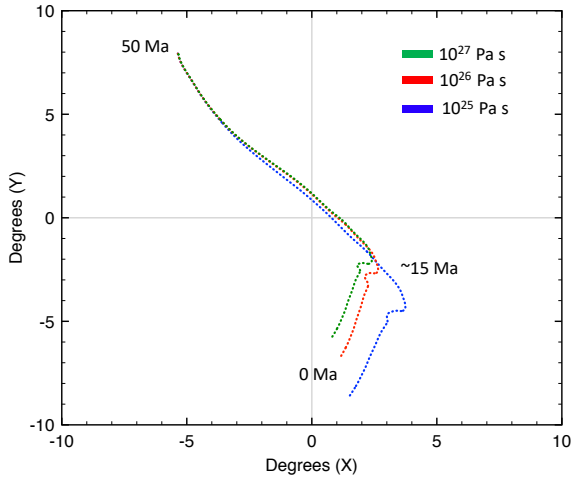

Fig. 3: Predicted convection-driven TPW paths. Results are shown for TPW calculations in which the adopted viscosity of the lithosphere is varied (as labeled). The path is shown for a cartesian co-ordinate system centered on the north pole in which X and Y axes are in the directions of 0°E and 90°E

The final pole positions in the three TPW time series are not coincident with the present-day pole and this raises an interesting issue. Steinberger and O'Connell (1997) and Adhikari et al. (2018) enforce a present-day pole position by adding a constant shift in the geopotential to match the present-day position. However, this approach is equivalent to imposing a fixed

perturbation to the inertia tensor across the entire time series, which will have the effect of altering the stabilization of the pole by changing the background excess ellipticity of the Earth in a manner inconsistent with the prediction of the convection simulation. (Whether that stabilization is decreased or increased - i.e., predicted TPW rates increase or decrease, respectively - will depend on the sign of the perturbation to the excess ellipticity.) We have found that applying a correction of this kind decreases our predicted TPW rates, but do not believe that such a correction is justifiable. A more rigorous approach would be to run many adjoint-based convection simulations and search for the subset that predict a present-day pole position "closest" to the observed location, but given the numerical cost of doing so (see Methods) we leave this effort to future work. In any case, the displacement of the predicted present-day pole positions in Fig. 3 from the observed location are relatively small (e.g., less than 6° for the case of a lithospheric viscosity of 10^{27} Pa s), which reflects the fact that the adjoint simulations are constrained to fit the present-day long wavelength geoid.

We turn next TPW driven by GIA. Ongoing polar wander (or motion) associated with remnant isostatic adjustment following the last ice age is sensitive to the broad geographic distribution of ice mass flux and its evolution from the Last Glacial Maximum (LGM) to the Holocene. To explore the uncertainty associated with history, we consider predictions of TPW based on two independent, global models of ice history across the last glacial cycle, ICE-6G (Peltier et al., 2015) and a model developed at ANU (Lambeck et al., 2014). Predictions of present-day TPW are computed using the viscosity model of Figure 2 and the rotational stability theory of Mitrovica et al. (2005) are shown in Figure 1 (blue and red circles). The time scale of ice age loading is much faster than the decay time of the lowest viscosity lithosphere considered in the convection simulations (as noted above, ~5 Myr for the case of 10^{25} Pa s), and thus calculations based on any of the viscoelastic lithospheres are essentially identical. The GIA predictions are insensitive to the choice of ice history. The two calculations yield magnitudes that are ~76% of the observed TPW rate with a direction of ~75°W, i.e., toward the location of the Laurentide Ice Sheet that dominated the excess ice budget at LGM. Moreover, the sum of the convection and GIA signals (blue and red filled ovals) falls within the observed 20th century rate after correction

for the signal for modern melting of polar ice sheets and glaciers (dashed black oval). As a final note, we also repeated the calculations using a recent viscosity model constrained to fit a range of GIA observations (Lau et al., 2017) and found that the magnitude of TPW rates shown in Fig. 1 (blue and red circles) are decreased by less than ~4%.

Conclusions

We conclude that the signal of ongoing GIA dominates the budget of modern TPW. Convection-induced TPW is governed by long-wavelength deep mantle buoyancy structure and in particular the density anomalies associated with the two Large Low Shear Velocity Provinces (LLSVPs) at the base of the mantle below southern Africa and the southwest Pacific (e.g., Ritsema et al., 2011; McNamara, 2019). Our mapping of seismic to density heterogeneity assumes that the former is due to purely temperature effects, but there is evidence that these structures involve significant compositional heterogeneity (e.g., Forte & Mitrovica, 2001; Lau et al., 2017; McNamara, 2019), and in this case we have likely overestimated the buoyancy of the LLSVPs. Thus, we interpret our estimate that the convection signal has a magnitude ~25-30% of the observed 20th century rate of TPW to be an upper bound. Indeed, a reduction of this signal by a factor of two, consistent with long term rates of TPW (Greff-Lefftz, 2004; Rouby et al., 2010; Chan et al., 2011), can be accommodated while preserving a fit to the observed rate. In future work we will extend the convection analysis described herein to incorporate the influence of compositional heterogeneities within an adjoint methodology (Ghelichkhan and Bunge, 2018) and to run a larger set of such simulations.

Methods

Adjoint Based Reconstructions of Cenozoic Mantle Dynamics and Structure

Sia – summarize the adjoint approach here. Emphasize the numerical cost (which would support comments about "future work" in the main text) and quantify the achieved fits to the present-day observations – something we mention in the main text

Rotational Stability Theory

With few exceptions, predictions of TPW driven by mantle convection adopt the equilibrium (i.e., final state) theory of Gold (1955) and Goldreich & Toomre (1969) in which there is no long-term stabilization of the Earth's rotation axis (e.g., Adhikari et al., 2018). Ricard et al. (1993) extended the rotational equilibrium (i.e., final state) theory of Gold (1955) and Goldreich & Toomre (1969) to incorporate time dependence in TPW associated with the delayed, viscoelastic adjustment of the rotational bulge. This rotational stability theory has been extended further to incorporate a stabilization mechanism (the so-called "remnant bulge") first described by Willemann (1984) associated with stresses in an elastic lithosphere that arise from the adjustment of the bulge (Matsuyama et al., 2006; Creveling et al., 2012; Harada, 2012, Chan et al., 2014). These elastic stresses introduce a memory of an initial pole position. An additional extension, by Moore et al. (2017), treats the case of a viscoelastic lithosphere. On time scales much shorter than the viscous relaxation time of the lithosphere, the polar motion computed using the Moore et al. (2017) theory follows the elastic lithosphere case, whereas on time scales much longer than the relaxation time of the lithosphere, the calculations converge to those computed using the time dependent stability theory of Ricard et al. (1993). Our calculations of convection-induced TPW are based on the treatment of Moore et al. (2017; Eqn. 12). All Earth models adopt the elastic and density structure of the seismic model PREM (Dziewonski & Anderson, 1981) and the viscosity profile shown in Figure 2. The three Earth models are distinguished on the basis of the viscosity of the lithosphere (10^{25} Pa s, 10^{26} Pa s, and 10^{27} Pa s) which establishes the relaxation time of the lithosphere – and thus the time scale over which any reorientation of the rotation axis is stabilized by the remnant bulge in the presence of the convective driving force.

References

Adhikari, S., Caron, L., Steinberger, B., Reager, J. T., Kjeldsen, K. K., Marzeion, B., Larour, E., & Ivins, E. R. What drives 20th century polar motion? *Earth Planet. Sci. Lett.*, 502, 126–132 (2018).

Argus, D. F., & Gross, R. S. An estimate of motion between the spin axis and the hotspots over the past century, *Geophys. Res. Lett.* , 31**,** L06614, doi:10.1029/2004GL019657 (2004).

Chan, N.-H., Mitrovica, J. X., Matsuyama, I., Latychev, K., Creveling, J. R., Stanley, S., & Morrow, E. The rotational stability of a convecting Earth: The Earth's figure and TPW over the last 100 Myr, *Geophys. J. Int.,* 187, 773–782, 2011.

Chan, N.-H., Mitrovica, J. X., Daradich, A., Creveling, J. R., Matsuyama, I., & Stanley, S. Time-dependent rotational stability of dynamic planets with elastic lithospheres, *J. Geophys. Res. - Planets*, 119, 169–188 (2014).

Creveling, J. R., Mitrovica, J. X., Chan, N.-G., Latychev, K., & Matsuyama, I. Mechanisms for oscillatory true polar wander, *Nature*, 491, 244–248 (2012).

Dziewonski, A.W., & Anderson, D. Preliminary Reference Earth Model, *Phys. Earth Planet. Int.*, 25, 297-356 (1981).

Forte, A.M., & Mitrovica, J.X. High viscosity deep mantle flow and thermochemical structure inferred from seismic and geodynamic data", *Nature*, 410, 1049-1056 (2001).

Ghelichkhan, S., & Bunge, H.-P. The compressible adjoint equations in geodynamics: Derivation and numerical assessment, *Int. J. Geomath.*, 7, 1–30 (2016).

Ghelichkhan, S., Bunge, H.-P. The adjoint equations for thermochemical compressible mantle convection: Derivation and verification by twin experiments, *Proc. Roy. Soc. A*, 474, 20180329, doi:10.1098/rspa.2018.0329 (2018).

Ghelichkhan, S., Bunge, H.-P. Global mantle flow retrodictions for the early Cenozoic using an adjoint method: evolving dynamic topographies, deep mantle structures, flow trajectories and sublithospheric stresses, *Geophys. J. Int.*, in review (2021).

Gold, T. Instability of the Earth's axis of rotation, *Nature*, 175, 526–529 (1955).

Goldreich, P., & Toomre, A. Some remarks on polar wandering, *J. Geophys. Res.*, 74, 2555–2567 (1969).

Greff-Lefftz, M. Upwelling plumes, superswells and true polar wander, *Geophys. J. Int.,* 159, 1125–1137 (2004).

Harada, Y. Long-term polar motion on a quasi-fluid planetary body with an elastic lithosphere: semi-analytic solutions of the time-dependent equation, *Icarus*, 220, 449–465 (2012).

Kjeldsen, K., et al. Spatial and temporal distribution of mass loss from the Greenland Ice Sheet since AD 1900, *Nature*, 528, 396–400 (2015).

Lambeck, K., Rouby, H., Purcell, A., Sun, Y., & Sambridge, M. Sea level and global ice volumes from the Last Glacial Maximum to the Holocene, *Proc. Natl. Acad. Sci. U.S.A.,* 111, 15296-15303 (2014).

Lau, H.C.P., Mitrovica, J.X., Davis, J.L., Tromp, J., Yang, H.-Y., & al-Attar, D. Tidal tomography constrains Earth's deep mantle buoyancy, *Nature*, 551, 321-326 (2017).

Matsuyama, I., Mitrovica, J.X., Perron, J.T., Manga, M., & Richards, M.A. Rotational stability of dynamic planets with elastic lithospheres, *J. Geophys. Res.,* 111, 10.1029/2005JG002447 (E02003, P. 1-18), 2006.

Marzeion, B., Laclercq, P., Cogley, J., & Jarosch, A. Brief communication: global reconstructions of glacier ma ass change during the 20th century are consistent, *Cryosphere,* 9, 2399–2404 (2015).

McNamara, A.K. A review of large low shear velocity provinces and ultra low velocity zones, *Tectonophys.,* 760, 199-220 (2019).

Mitrovica, J. X., & Forte, A. M. A new inference of mantle viscosity based upon joint inversion of convection and glacial isostatic adjustment data, *Earth Planet. Sci. Lett.*, 225, 177–189 (2004).

Mitrovica, J. X., Hay, C. C., Morrow, E. Kopp, R. E., Dumberry, M. & Stanley, S. Reconciling past changes in Earth rotation with 20th century global sea-level rise: Resolving Munk's enigma, *Science Adv.*, 1, doi: 10.1126/sciadv.1500679 (2015).

Mitrovica, J. X., Wahr, J. M., Matsuyama, I., & Paulson, A. The rotational stability of an ice-age Earth, *Geophys. J. Int.*, 161, 491–506 (2005).

Moore, K., Chan, N.-H., Daradich, A., & Mitrovica, J. X. Time dependent rotational stability of planets with viscoelastic lithospheres, *Icarus*, 289, 34–41 (2017).

Munk, W. Twentieth century sea level: An enigma, *Proc. Nat. Acad. Sci.*, 99, 6550-6555 (2002).

Peltier, W. R., Global sea level and Earth rotation, *Science*, 240, 895–891 (1988).

Peltier, W.R., Argus, D.F., & Drummond, R. Space geodesy constrains ice age terminal deglaciation: The global ICE-6G_C (VM5a) model, *J. Geophys. Res.: Solid Earth,* 120, 450-487 (2015).

RGI Consortium. Randolph Glacier Inventory – A Dataset of Global Glacier Outlines: Version 6.0: Technical Report, Global Land Ice Measurements from Space, Colorado, USA. Digital Media. DOI: https://doi.org/107265/N5-RGI-60 (2017).

Ricard, Y., Spada, G., & Sabadini, R. Polar wandering of a dynamic Earth, *Geophys. J. Int.*, 113, 284–298 (1993).

Richards, M. A., Ricard, Y., Lithgow-Bertelloni, C., Spada, G., & Sabadini, R. An explanation for Earth's long-term rotational stability, *Science*, 275, 372–375 (1997).

Richards, M. A., Bunge, H.-P., Ricard, Y., & Baumgardner, J. R. Polar wandering in mantle convection models, *Geophys. Res. Lett.*, 26, 1777–1780 (1999).

Ritsema, J., Deuss, A., van Heijst, H. J., & Woodhouse, J. H. S40RTS: a degree-40 shear-velocity model for the mantle from new Rayleigh wave dispersion, teleseismic traveltime and normal-mode splitting function measurements, *Geophys. J. Int*., 184, 1223–1236 (2011).

Rouby, H., Greff-Lefftz, M., & Besse, J. Mantle dynamics, geoid, inertia and TPW since 120 Myr, *Earth Planet. Sci. Lett.*, 292, 301–311 (2010).

Sabadini, R., & Peltier, W. R. Pleistocene deglaciation and the Earth's rotation: implications for mantle viscosity, *Geophys. J. R. astr. Soc.*, 66, 553–578 (1981).

Sabadini, R., Yuen, D. A., & Boschi, E. Polar wandering and the forced responses of a rotating, multilayered, viscoelastic planet, *J. Geophys. Res*, 87, 2885 (1982).

Steinberger, B., & O'Connell, R. J. Changes of the Earth's rotation axis owing to the advection of mantle density anomalies, *Nature*, 387, 169–173 (1997).

Steinberger, B., & Torsvik, T. H. Absolute plate motions and true polar wander in the absence of hotspot tracks, *Nature*, 452, 620–623 (2008).

Steinberger, B., & Torsvik, T. H. Toward an explanation for the present and past locations of the poles, *Geochem. Geophys. Geosys.,* 11, doi:1029/2009GC002889 (2010).

Su, W., Woodward, R. L., & Dziewonski, A. M. Degree 12 model of shear velocity heterogeneity in the mantle, *J. Geophys. Res.,* 99, 6945–6980 (1994).

Willemann R. J. Reorientation of planets with elastic lithospheres, *Icarus*, 60, 701–709 (1984).

Wu, P., & Peltier, W. R. Pleistocene deglaciation and the Earth's rotation: a new analysis, *Geophys. J. R. astr. Soc.*, 76, 753–791 (1984).